JOURNAL OF combinatorial CHEMISTRY

Subscriber access provided by American Chemical Society

Report

A Method for Combinatorial Fabrication and Characterization of Organic/Inorganic Thin Film Devices in UHV

Stefan Egger, Seiji Higuchi, and Tomonobu Nakayama

J. Comb. Chem., **2006**, 8 (3), 275-279• DOI: 10.1021/cc0501662 • Publication Date (Web): 22 April 2006

Downloaded from http://pubs.acs.org on March 22, 2009

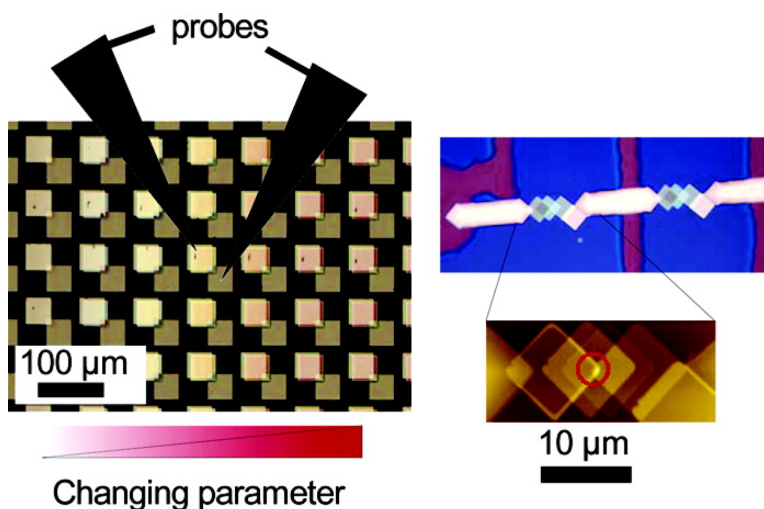

More About This Article

Additional resources and features associated with this article are available within the HTML version:

- Supporting Information
- Links to the 6 articles that cite this article, as of the time of this article download
- Access to high resolution figures
- Links to articles and content related to this article
- Copyright permission to reproduce figures and/or text from this article

View the Full Text HTML

ACS Publications
High quality. High impact.

Journal of Combinatorial Chemistry is published by the American Chemical Society.
1155 Sixteenth Street N.W., Washington, DC 20036

JOURNAL OF combinatorial CHEMISTRY

© Copyright 2006 by the American Chemical Society

Volume 8, Number 3 May/June 2006

Reports

A Method for Combinatorial Fabrication and Characterization of Organic/Inorganic Thin Film Devices in UHV

Stefan Egger,*,† Seiji Higuchi,‡ and Tomonobu Nakayama‡,§

International Center for Young Scientists and Nanomaterials Laboratory, National Institute for Materials Science, Tsukuba, Japan, and Graduate School of Applied and Pure Sciences, University of Tsukuba, Tsukuba, Japan

Received December 22, 2005

Using the dynamic shadow mask technique, one can fabricate clean structures in ultrahigh vacuum (UHV) with lateral dimensions down to the nanoscale. For this, a perforated membrane is moved with high precision in close proximity to the substrate during exposure to a molecular beam. After the earlier demonstration of the technique,[1−4] more powerful, dedicated instruments were recently developed.[5,6] The working principle of the dynamic shadow mask technique is compatible with the basic principles of combinatorial discovery: parallelization and variation.[7] In this work, we focus on the setup and general fabrication strategies of the dynamic shadow mask technique in combination with a combinatorial methodology.[7] As applications, we are targeting thin film devices incorporating organic material. Such structures have high potential in electronics and optoelectronics. With this approach, in addition to being able to choose among a large number of potentially suitable molecules, one can tune the device properties by changing other parameters, such as doping, film thickness, and crystalline order.[8,9] A further crucial problem is the connection to metallic or semiconducting electrodes.[10,11] The interface between the electrodes and the active layer(s) has to have the right electronic and chemical properties[8−10] and needs to be thermally[12] and mechanically[13] stable. Fabricating structures in UHV offers the best possible control over the composition.[9] Systematic studies under such well-defined conditions may be crucial, even in cases in which the long-term goal is to have a cheaper fabrication method for mass production.[14] The additional ability of fabricating structures with lateral dimensions in the nanometer range provides better access to single crystalline layers with no defects and allows one to prototype devices with high density and high speed.

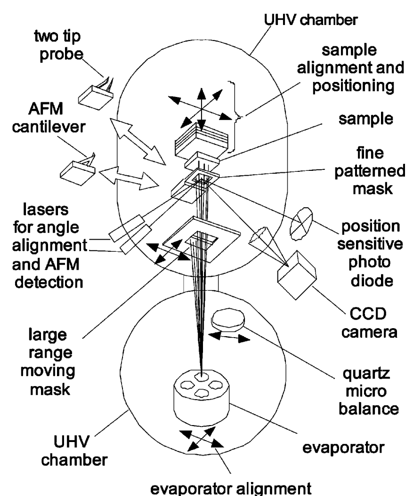

Figure 1. Schematic diagram of the setup. The approximate lengths are distance sample to fine mask, 1 μm (or larger, depending on the required edge definition and mask type); distance sample to large mask, 2 mm; and distance sample to evaporator, 20 cm.

In Figure 1, a schematic overview of the setup is shown. It consists of four main parts: (i) the material source; (ii) a large shadow mask that acts as a shutter with continuous lateral movement for "global" variation[15] of device properties over the whole sample; (iii) a fine-patterned shadow mask

* Corresponding author. E-mail: egger.stefan@nims.go.jp.
† International Center for Young Scientists, National Institute for Materials Science.
‡ University of Tsukuba.
§ Nanomaterials Laboratory, National Institute for Materials Science.

10.1021/cc0501662 CCC: $33.50 © 2006 American Chemical Society
Published on Web 04/22/2006

for the definition of arrays of devices; and (iv) an ultra precise positioning unit which moves the sample in close proximity to the mask, with a gap that can be as small as 1 μm. These main components are briefly described as follows (additional information can be found in ref 5):

(i) The material source is a commercial, multiple-crucible e-beam evaporator,[16] modified with resistive heated crucibles for organic materials and additional getter sources for alkali metals. The evaporation rate is calibrated with a quartz microbalance.[17] Numerous metals, insulators and (organic) semiconductors can be evaporated.

(ii) The "global" shadow mask is actuated by a solenoid. Static friction is avoided by using a flexure design. With this design, the relation between the current in the solenoid and the position of the "global" mask is stable and was calibrated and checked in situ with a CCD camera. Currently, this mask allows variation of the exposure in one direction. With a more sophisticated design,[15] variations in two dimensions can be obtained.

(iii) Different types of fine patterned masks were employed: focused ion beam patterned silicon nitride membranes[18] and commercially available electron microscopy grids.[19] The masks, mounted on holders, can be exchanged using a UHV manipulator. Electrical two-point probes or scanning probe microscopy tips can be attached to similar holders, as shown in Figure 1, for in-situ characterization of fabricated structures.

(iv) The sample positioning unit consists of several different components to combine high accuracy and mechanical stiffness with experimental flexibility. In our setup, the fine-patterned mask is fixed, and the sample moves. A commercial flexure stage with absolute position sensor[20] allows high-precision movements in the directions parallel to the substrate surface (resolution, 0.3 nm; full-range repeatability, 3 nm; range, 100 μm). An additional custom-built inertial slider stage[21] extends the travel range to 6×6 mm^2. In the vertical direction, a linear motor[22] and a piezo ceramic tube are used for coarse and fine travel, respectively, to approach the sample to the mask. A custom-built tilting inertial slider allows angle alignment of the substrate surface relative to the mask with an accuracy of some tens of microradians.

The components are located in a UHV system with base pressure below 1×10^{-9} mbar, and which is mounted on vibration isolations. All in vacuo parts can be baked up to 150 °C. An Ar^+ sputtering gun and an annealing stage are available for sample preparation. The fabrication of structures is done fully automatically through dedicated software.

Compared to a static mask, the ability to precisely control the motion of the shadow mask gives a significant increase in the number of possible geometries. Interesting structures can be generated even by using a very simple patterned mask. As an example, we chose a mask with square apertures to create an entire device. First, the bottom electrode is grown, then the mask is moved sequentially at different positions[23] to grow the active layer(s), followed by the top electrode and, if necessary, an additional insulating capping layer. Figure 2 shows schematically how the different layers are positioned relative to each other in the device. If the active layer has a much lower conductivity, as is the case in general when using organic interlayers and metallic electrodes, then the active part of the device is localized in the overlapping region of the two electrodes (dotted circle in Figure 2). The remaining area of the electrodes serves as connection pads. As an additional advantage of the moving shadow mask technique, the edges can be smoothed to avoid kinks in the overlapping region, thus decreasing potential field enhancement effects. This is done by moving the mask during deposition or by increasing the mask−substrate distance. Note that the device area can be fabricated much smaller than the mask apertures because it depends mainly on the positioning accuracy. With this strategy, the use of very small apertures, which tend to clog rapidly,[2] can be avoided.

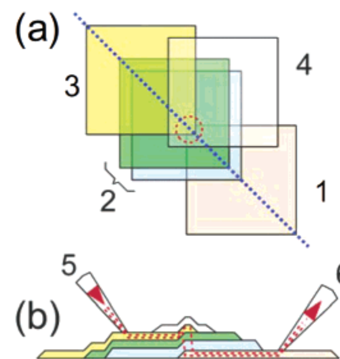

Figure 2. Layout of a thin film device fabricated with a square aperture. (a) Top view. Different materials are evaporated at different mask positions: (1) bottom electrode, (2) layer(s) of active material, (3) top electrode, and (4) optional capping layer for device protection. (b) Cross section of (a) (along the dotted blue line in (a)) with probes for electrical measurements (5, 6). The current passes through the active layers in the small overlapping electrode area, indicated by the red dotted lines in (b) and circle in (a). The edges of the active area can be tempered to minimize field enhancement effects.

To apply a combinatorial methodology, we used a large array of apertures of the type described above, together with a second "global" shadow mask that was moved over the whole array area. This global mask allows one to vary one or two parameters[7] over the device array and so to generate structures for an entire device library. The variation can involve the active layer (its thickness, doping level, or mixtures of different molecules), the electrodes (to alloy their composition or to change their work function and chemical interaction), or the capping layer. An example of such an array of devices, in which one parameter was varied, is shown in Figure 3. In this example, commercially available electron microscopy grids[24] were used. The overlapping region, corresponding to the circle in Figure 2, is 11 μm wide, which is a suitable size for investigations of properties of continuous films and allows one to reduce the influence of defects.

To grow smaller structures, more precise masks with very well-defined edges are necessary. Silicon nitride membranes, supported by a Si frame, are suitable starting substrates for this purpose. These membranes are flat to within nanometers and can be cut with nanometer precision by focused ion beam (FIB) or electron beam lithography.[1,2] In this work, FIB was used due to its flexibility and ease of use. Two examples of devices made with such masks are shown in Figure 4. In

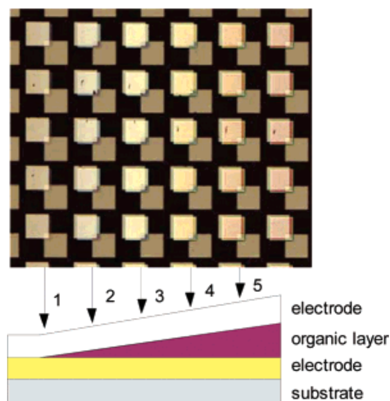

Figure 3. Array of Ti/C_{60}/Ti structures on a quartz substrate, fabricated as outlined in Figure 2 (without capping layer), using an array of squares as a shadow mask. A global shadow mask was used to create a linear variation of the thickness of the C_{60} layer, from 10 to 90 nm. The size of the square electrodes is 60 × 60 μm^2; the size of overlapping region is 11 × 11 μm^2.

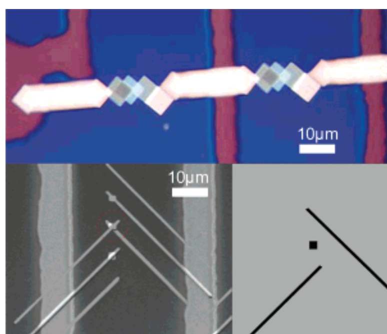

Figure 4. Examples of electrically connected devices fabricated using FIB patterned silicon nitride membrane masks. (a) Two devices formed using 6-μm square apertures. (b) C_{60} island sandwiched between crossing metal lines (marked with a dotted circle). The structure was fabricated in three steps using a stencil with FIB cuts as outlined in (c). The devices in (a) and (b) are further connected using larger metal lines (vertical stripes) to bonding pads (not shown). All the elements of the structures, including the large connecting lines and pads, were fabricated in situ.

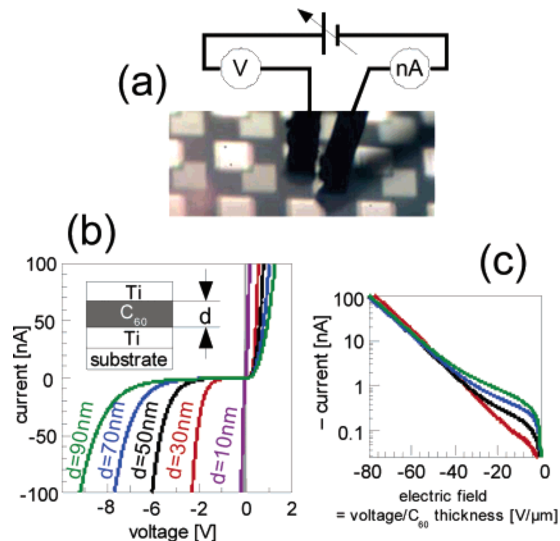

Figure 5. Electrical transport measurements on the sample array from Figure 3 (Ti/C_{60}/Ti/quartz, structures fabricated at room temperature). (a) Two-point probe on device pads. (b) I−V characteristics of different devices with different C_{60} thicknesses. (c) I−V characteristics from (b) plotted as a function of the average electric field in the device. At high fields, an exponential behavior with the electric field is obtained. (For small voltages, the resistivity of the C_{60} is $\sim 10^{-8}$ Ωcm.)

Figure 4a we used the same strategy with overlapping regions, as described above, but on a smaller scale. In Figure 4b, a different principle is applied: the combination of different shapes generated by different parts from the same stencil mask. This strategy extends the possible device geometries. Complex devices can be assembled from several components. In both cases, the structures were electrically connected with larger wires to bonding pads. These large patterns were fabricated in-situ with separate, micrometer-scale patterned stencils.

To characterize structures in UHV, a large range of suitable techniques could be applied. In the following, we will focus on some in-situ characterization methods that can be easily implemented using the same components as those used for fabrication. For electrical transport measurements, a two-point probe was constructed. It consists of two 50-μm-diameter palladium wires, with a spacing that fits on the square patterns shown in Figures 2 and 3. This probe, mounted on an adaptor with electrical connections, replaces the fine-patterned mask (Figure 1). In this way, the probe is very easy to use; since the wires are flexible, scratching of the connection pads that can affect the electrical connections is not an issue. Moving from one device to the next takes a few seconds. This is done manually, using an optical microscope with a CCD camera (automating this procedure did not seem appropriate, although this can be implemented). Figure 5a shows the image of the two-point probe connecting a device in the array, which was recorded from the CCD camera.

As an example of the application of the techniques described above, we investigated the properties of a thin film device array of the type shown in Figure 3. This consists of a C_{60} film of variable thickness sandwiched between Ti electrodes. Ti evaporated over C_{60} is known to interact strongly with fullerenes and can lead to titanium carbide formation.[25,26] Even at room temperature, ~0.2 fullerene layers are disrupted in the carbide formation.[25,26] This effect is increased at higher temperatures. Figure 5b shows I−V characteristics obtained for both voltage polarities, with the bias applied to the top electrode while the bottom electrode was grounded. Although both electrodes are made of Ti, the two interfaces with the C_{60} film have asymmetric behavior: one is closer to ohmic behavior; the other one indicates the formation of a barrier for carrier injection. To allow for the identification of the blocking interface, a second sample array was fabricated. In this array, the thickness of the C_{60} film was kept constant to an intermediary thickness of 45 nm, whereas the thickness of the top Ti electrode was varied from 0 to ~1.2 nm. This top Ti layer of variable thickness was followed by a Au layer of constant thickness, ~12 nm. Figure 6 shows I−V characteristics taken on this second array. The characteristics changed considerably with varying thickness of the Ti layer and, thus, indicate the formation of a blocking interface induced by depositing Ti on top of the C_{60} film. Figure 6 also demonstrates that the blocking interface in the first array of devices, from Figure 5, is the top one. We propose that this blocking interface is caused by the partial

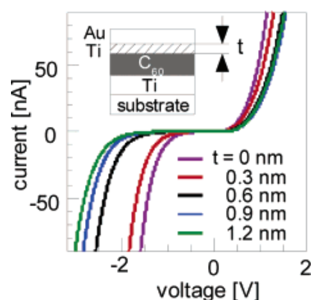

Figure 6. I−V measurements on Au/Ti/C_{60}/Ti/quartz structures at different thicknesses of the top Ti layer. The C_{60} film is 45 nm thick. I−V curves of devices show increasingly asymmetric transport characteristics with an increase in the top Ti layer thickness.

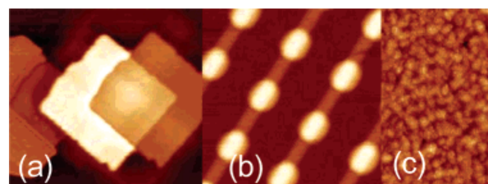

Figure 7. nc-AFM images recorded in-situ. (a) Device formed by a square aperture. The electrode overlap area is ~200 nm wide (a mask with unusual rough edge was used). The interlayer is made of C_{60}. Image size, 12 × 12 μm^2; height range, 53 nm. (b) Test structure with CaF_2 dots on Ti lines. Image size, 3 × 3 μm^2; height range, 18 nm. (c) Grain structure of Au on quartz (image size, 600 × 900 nm^2; height range, 12 nm).

disruption of the top C_{60} layer due to carbide formation.[25,26] This leads to the modification of the top electrode, which now contacts the next intact molecular layer of C_{60}. The mechanism causing this blocking interface is unclear, and additional characterization is necessary for a better understanding. In-situ Kelvin probe microscopy recently implemented in the system will allow quantifying the changes in the work function of this reacted interface. The work function of the interface is one of the parameters controlling the injection into the C_{60} bulk layer. To our knowledge, the electrical transport across the Ti/C_{60} interface was not studied previously, but a remarkably similar case of rectifying behavior was observed in Al/C_{60}/Al diodes.[27] In this case, it was found that to change the injection regime from rectifying to ohmic, it was necessary to insert additional LiF layers between the layer of Al and C_{60}.[27]

Since in Figure 5 the blocking behavior is obtained when the top electrode is negatively biased, it follows that the C_{60} film behaves as an n-type semiconductor, in agreement with FET-based measurements of the type of the majority carrier in such a film.[28] Figure 5c shows the same I−V data for negative bias as shown in Figure 5b, but plotted as a function of the average field in the device (defined as the ratio between the applied bias and the C_{60} film thickness). The I−V characteristics for all the C_{60} film thicknesses superpose at high field values (Figure 5c), whereas at low field, there is a dependence on this thickness. This behavior indicates that at high fields, the electric transport is dominated by carrier injection over the barrier formed at the top interface. On the other hand, at low fields, the current is related to a region depleted of mobile charges that extends from the top interface inside the bulk of the C_{60} film. In this latter case, the current is probably due to a mechanism of field-assisted thermal generation in this depleted region; hence, the thickness dependence of the I−V characteristics. Further characterization, such as I−V measurements at variable temperature, is needed to characterize the two interfaces and elucidate the reasons for their unexpected asymmetry.

An additional in-situ characterization method implemented by using essentially the same setup is scanning probe microscopy (SPM), and examples of images recorded in situ are shown in Figure 7. Even if SPM for the characterization of a large array of structures may often be time-consuming, the characterization of selected objects can provide necessary knowledge about topography, nanoscale conductivity, and surface potential. The high-precision positioning unit used in this system is well-suited for performing SPM. The closed-loop, fine-positioning stage allows drift-free imaging, which is convenient (and time-efficient) when moving to different positions or when changing the scanning range abruptly. Several different modes of atomic force microscopy (AFM) and scanning tunneling microscopy can be used, including noncontact atomic force microscopy (nc-AFM). In this latter mode, the resonance frequency change of the lever[29] is detected using commercial electronics.[30] The nc-AFM technique allows fast scanning without damaging fragile structures. Additionally, nc-AFM can be easily extended to perform Kelvin probe microscopy to characterize surface potential distributions; this is important for the understanding of interface formation.

In conclusion, we have presented a highly flexible UHV fabrication and in-situ characterization method which allows one the use of efficient strategies as established in combinatorial discovery. Straightforward applications involve organic/metallic (or organic/semiconducting) multilayer devices.

Acknowledgment. We thank Prof. Mark E. Welland for his support and we thank Dr. Adelina Ilie and Mr. Masato Nakaya for helpful discussions. This work was funded through the Special Coordination Funds for Promoting Science and Technology from the Ministry of Education, Culture, Sports, Science and Technology of the Japanese Government.

References and Notes

(1) Ono, K.; Shimada, H.; Kobayashi, S. I.; Ootuka, Y. *Jpn. J. Appl. Phys. Part 1* **1996**, *35* (4A), 2369−2371.
(2) Deshmukh, M. M.; Ralph, D. C.; Thomas, M.; Silcox, J. *Appl. Phys. Lett.* **1999**, *75* (11), 1631−1633.
(3) Luthi, R.; Schlittler, R. R.; Brugger, J.; Vettiger, P.; Welland, M. E.; Gimzewski, J. K. *Appl. Phys. Lett.* **1999**, *75* (9), 1314−1316.
(4) Champagne, A. R.; Couture, A. J.; Kuemmeth, F.; Ralph, D. C. *Appl. Phys. Lett.* **2003**, *82* (7), 1111−1113.
(5) Egger, S.; Ilie, A.; Fu, Y. T.; Chongsathien, J.; Kang, D. J.; Welland, M. E. *Nano Lett.* **2005**, *5* (1), 15−20.
(6) Zahl, P.; Bammerlin, M.; Meyer, G.; Schlittler, R. R. *Rev. Sci. Instrum.* **2005**, *76* (2), 023707.
(7) Xiang, X. D.; Sun, X. D.; Briceno, G.; Lou, Y. L.; Wang, K. A.; Chang, H. Y.; Wallacefreedman, W. G.; Chen, S. W.; Schultz, P. G. *Science* **1995**, *268* (5218), 1738−1740.
(8) Barlow, S. M.; Raval, R. *Surf. Sci. Rep.* **2003**, *50* (6−8), 201−341.

(9) Dimitrakopoulos, C. D.; Malenfant, P. R. L. *Adv. Mater.* **2002**, *14* (2), 99.
(10) Zhu, X. Y. *Surf. Sci. Rep.* **2004**, *56* (1−2), 1−83.
(11) Basch, H.; Cohen, R.; Ratner, M. A. *Nano Lett.* **2005**, *5* (9), 1668−1675.
(12) Durr, A. C.; Schreiber, F.; Kelsch, M.; Carstanjen, H. D.; Dosch, H. *Adv. Mater.* **2002**, *14* (13−14), 961.
(13) Mammeri, F.; Le Bourhis, E.; Rozes, L.; Sanchez, C. *J. Mater. Chem.* **2005**, *15* (35−36), 3787−3811.
(14) This report focuses only on structures entirely fabricated in UHV, but some of the described strategies could be adapted for studies on films previously grown ex situ, in a top-contacted FET-type geometry.
(15) Takahashi, R.; Kubota, H.; Murakami, M.; Yamamoto, Y.; Matsumoto, Y.; Koinuma, H. *J. Comb. Chem.* **2004**, *6* (1), 50−53.
(16) EGC04, Oxford Applied Research, UK.
(17) XTM/2, Inficon, U.S.A.
(18) Kim, G. M.; van den Boogaart, M. A. F.; Brugger, J. *Microelectron. Eng.* **2003**, *67−8*, 609−614.
(19) Athene Old 200, Agar Scientific, UK. (Two grids were combined to decrease the square aperture size to 60 μm.)
(20) P-733.2UD, PI, Germany.
(21) Pohl, D. W. *Rev. Sci. Instrum.* **1987**, *58* (1), 54−57.
(22) UHVL-025, Burleigh Instruments, Plano, TX.
(23) When describing the sample/mask relative motions during structure fabrication, we treat the sample substrate as static, but in the actual setup, the sample is moved, and the fine-patterned mask is kept in a fixed position.
(24) Athene Old 200, Agar Scientific, UK. (Two grids were combined to decrease the square aperture size to 60 μm.)
(25) Ohno, T. R.; Chen, Y.; Harvey, S. E.; Kroll, G. H.; Benning, P. J.; Weaver, J. H.; Chibante, L. P. F.; Smalley, R. E. *Phys. Rev. B* **1993**, *47* (4), 2389−2393.
(26) Wang, W. H.; Wang, W. K. *J. Appl. Phys.* **1996**, *79* (1), 149−152.
(27) Feng, X. D.; Huang, C. J.; Lui, V.; Khangura, R. S.; Lu, Z. H. *Appl. Phys. Lett.* **2005**, *86* (14), 143511.
(28) Haddon, R. C.; Perel, A. S.; Morris, R. C.; Palstra, T. T. M.; Hebard, A. F.; Fleming, R. M. *Appl. Phys. Lett.* **1995**, *67* (1), 121−123.
(29) Albrecht, T. R.; Grutter, P.; Horne, D.; Rugar, D. *J. Appl. Phys*. **1991**, *69* (2), 668−673.
(30) EasyPLL plus, Nanosurf, Switzerland.

CC0501662